



OPEN

Integrated single cell and bulk RNA sequencing analyses reveal the impact of tryptophan metabolism on prognosis and immunotherapy in colon cancer

Yanyan Hu^{1,2}, Ximo Xu^{1,2}, Hao Zhong^{1,2}, Chengshen Ding¹, Sen Zhang¹, Wei Qin¹, Enkui Zhang¹, Duohuo Shu¹, Mengqin Yu¹, Naijipu Abuduaini¹, Xiao Yang¹✉, Bo Feng¹✉ & Jianwen Li¹✉

Tryptophan metabolism is intricately associated with the progression of colon cancer. This research endeavored to meticulously analyze tryptophan metabolic characteristics in colon cancer and forecast immunotherapy responses. This study analyzed colon cancer samples from a training cohort of 473 tumors and 41 normal tissues from TCGA, with validation in 902 cancer patients across multiple GEO datasets. Patients were stratified into subtypes through consistent clustering, and a tryptophan metabolic risk score model was constructed using the random forest algorithm. Based on these risk scores, patients were delineated into high and low-risk groups, and their clinicopathologic characteristics, immune cell infiltration, immune checkpoint expression, and signaling pathway disparities were examined. The Oncopredict algorithm facilitated the identification of sensitive chemotherapeutic agents, while the immune escape score was employed to evaluate the immunotherapy response across risk groups. Transcriptomic sequencing findings were corroborated by single-cell sequencing from Shanghai Ruijin Hospital. Two distinct subtypes of colon cancer patients emerged, exhibiting significant prognostic and immune cell infiltration differences. The high-risk group demonstrated a poorer prognosis ($p < 0.001$), advanced clinical stage ($p < 0.001$), and elevated immunosuppressive cell expression ($p < 0.05$). Additionally, three chemotherapeutic drugs showed efficacy in the high-risk cohort, displaying a heightened immune escape potential ($p < 0.05$) and diminished response to immunotherapy. Single-cell sequencing validated the overexpression of tryptophan-related genes in epithelial cells. In conclusion, tryptophan metabolism significantly influences the colon cancer immune microenvironment, with high-risk patients experiencing adverse prognoses and potentially reduced efficacy of immunotherapy.

Keywords Colon cancer, Tryptophan metabolism, Risk score, Prognosis, Immunotherapy

Abbreviations

CC	Colon cancer
CRC	Colorectal cancer
COAD	Colon adenocarcinoma
TMGs	Tryptophan metabolic related genes
RF	Random Forest
SVM	Support Vector Machine
scRNA-seq	Single cell RNA sequencing
Bulk-seq	Bulk sequencing
TCGA	The Cancer Genome Atlas
GEO	Gene Expression Omnibus

¹Department of General Surgery, Ruijin Hospital, Shanghai Jiao Tong University School of Medicine, Shanghai, China. ²Yanyan Hu, Ximo Xu, Hao Zhong are contributed equally to this paper and shared the first author. ✉email: yxrjmis@alumni.sjtu.edu.cn; fengbo2022@163.com; ljjw5@yeah.net

GDSC	Genomics of Drug Sensitivity in Cancer
MSigDB	The Molecular Signatures Database
R	R language
NKAIN4	Sodium/Potassium Transporting ATPase Interacting Protein4
TNNT1	Troponin T Type 1
PCOLCE2	Procollagen C-Endopeptidase Enhancer 2
SLC16A8	Recombinant Solute Carrier Family 16, Member 8
UPK3B	Human uroplakin 3b
timeROC	Time Receiver Operating Characteristic Curve
AUC	Area Under Curve
PCA	Principal Component Analysis
C-index	Concordance index
RMS	Restricted Mean Survival
TMB	Tumor mutational burden
MSI	Microsatellite instability
CNV	Copy number variations
TME	Tumor microenvironment
GO	Gene Ontology
KEGG	Kyoto Encyclopedia of Genes and Genomes
GSEA	Gene Set Enrichment Analysis
GSVA	Gene set variation analysis
TIDE	Tumor Immune Dysfunction and Exclusion
ICB	Immune checkpoint blockade
TISCH	Tumor Immune Single-cell Hub
scTIME	Single-Cell Analysis of the Immune Microenvironment
CDF	Cumulative Distribution Function
KM	Kaplan–Meier
T	Tumor
N	Node
M	Metastasis
HR	Hazard Rate
PD1	Programmed cell death protein 1
PDL1	Programmed cell death 1 ligand 1
CTLA4	Cytotoxic T-lymphocyte associated protein 4
Treg	Regulatory T cells
CAF	Cancer-Associated Fibroblasts
TME	Tumor Microenvironment

Metabolic reprogramming stands as a pivotal hallmark of cancer, where tumor cells adeptly alter their metabolic pathways to meet energy and biosynthetic demands, evading immune surveillance and therapeutic interventions^{1,2}. While amino acid metabolism plays an important role in supporting tumor growth, recent research has identified tryptophan metabolism as particularly relevant to cancer progression and immune modulation^{3,4}. Alterations in tryptophan pathways have been linked to diverse tumor behaviors and immune responses, drawing significant attention to its specific impact in cancers such as colon cancer (CC)^{5–7}.

Numerous investigations have unveiled the intricate involvement of tryptophan metabolic reprogramming within cancer milieu. In melanoma, activation of the kynurenine pathway orchestrated tumor progression and metastasis by modulating tumor microenvironment (TME) and enkindling angiogenesis⁸. In breast cancer, the overload of the serotonin pathway was believed to be associated with resistance to tamoxifen therapy⁹. In CC, metabolites of tryptophan acted as a driving factor in the progression of inflammatory bowel disease into CC¹⁰. Despite the above evidence, the comprehensive landscape of tryptophan metabolism in human CC remained vague^{11,12}. Major gaps in current research include the need to clarify how tryptophan metabolism affects CC patient prognosis, immune microenvironment dynamics, and therapeutic response¹³. Unraveling these complex patterns could deepen our understanding of cancer biology and inspire new therapeutic innovations¹⁴.

This study aims to comprehensively examine the expression profiles of tryptophan metabolism-related genes (TMGs) in CC at both bulk and single-cell levels to elucidate their potential oncogenic roles. By developing a predictive model based on TMG expression patterns, we sought to stratify patients into high- and low-risk groups, providing insights into prognosis and immune microenvironment characteristics. Furthermore, we aimed to identify targeted therapeutic options by screening potential drugs against key genes in high-risk samples, thereby contributing to the exploration of alternative therapeutic strategies for improved clinical outcomes in CC.

Materials and methods

Data source and processing

Transcriptome and clinical data were obtained from the Cancer Genome Atlas (TCGA) (<https://cancergenome.nih.gov/>) and Gene Expression Omnibus (GEO) (<https://www.ncbi.nlm.nih.gov/geo/>) databases^{15,16}. Raw transcriptomic data from TCGA were processed using the R package TCGAbiologics to download, normalize, and perform batch effect correction. GEO datasets were retrieved in their raw format and normalized using the limma package to ensure consistency across studies. The training cohort included 473 CC Samples and 41 normal tissues from TCGA-COAD. Validation encompassed 902 colorectal cancer (CRC) patients from

GSE38832 (n=122), GSE103479 (n=156), GSE39582 (n=585), GSE19862 (n=14) and GSE107797 (n=25). Tumor Immune Dysfunction and Exclusion (TIDE) database offered data on immune escape scores, while single-cell validation used GSE146771 (n=20), GSE179784 (n=4), and EMTAB8107 (n=7) from Tumor Immune Single-cell Hub (TISCH) database^{17,18}. For single-cell sequencing validation, tumor tissue samples (n=4) were gathered with written informed consent obtained from all subjects involved in the study. Ethical approval was secured from the Ethics Committee of Ruijin Hospital before sample collection. All experimental methods were performed in accordance with institutional and international ethical guidelines and regulations, as approved by the institutional ethics committee.

Subtypes analysis of cancer samples based on TMGs

We selected 40 genes associated with tryptophan metabolism from the MSigDB and Reactome databases, as these genes represent key components of tryptophan-related signaling pathways that have been implicated in cancer progression and immune modulation. Consensus clustering was performed using the “ConsensusClusterPlus” R package, chosen for its capacity to generate robust clusters by resampling and aggregating multiple clustering results. This technique is particularly valuable in cancer research as it improves the stability of identified subtypes, reducing variability often encountered in single clustering approaches¹⁹. 446 CC patients in the TCGA cohort were divided into two distinct clusters by the “Consensus Cluster +” R package. The survival prognosis of these clusters was analyzed using the “survival” R package. Principal component analysis (PCA) was utilized to visualize the clustered patients and assess the distinguishability of different subgroups. Two clusters were identified: Cluster 1, characterized by higher expression of genes involved in immune suppression pathways, and Cluster 2, associated with immune-active profiles, indicating distinct immunological landscapes within CC patients.

Construction and validation of a risk score model based on tryptophan metabolism

To construct a prognostic score based on tryptophan metabolism genes, differential analysis was performed on two tryptophan metabolism clusters. 873 differentially expressed genes were selected and among them, 16 genes were associated with survival. Random Forest (RF) and Support Vector Machine (SVM) machine learning algorithms were compared, with RF demonstrating strong diagnostic ability and stability^{20–22}. Cox regression analysis identified five signature genes for the risk model: NKA1N4 (Na⁺/K⁺ Transporting ATPase Interacting 4), TNNT1 (Troponin T Type 1), PCOLCE2 (Procollagen C-Endopeptidase Enhancer 2), SLC16A8 (Solute Carrier Family 16 Member 8), and UPK3B (Uroplakin 3B). The risk score integrated gene expression and the Cox regression coefficient. Median risk score split patients into high- and low-risk groups. Survival analysis and time-dependent receiver operating characteristic (timeROC) curves affirmed the model's significance and precision. Hazard distribution curves and PCA showcased group differences²³. The tryptophan metabolic risk score model was validated in both the TCGA-COAD internal training cohort and the external validation cohort including GSE38332, GSE103479, and GSE39582.

Correlation of the tryptophan metabolism risk score model with clinicopathological features

To assess the applicability of the tryptophan metabolic risk score model, survival analysis was conducted across various clinicopathological subgroups (T stage, N stage, M stage, and Pathological Stage). The model's performance was compared with other scoring models using metrics such as the concordance index (C-index) and Restricted Mean Survival (RMS). Moreover, a comparison was made between the model and previous studies by Hong²⁴, Wang²⁵, AHI²⁶, and Du²⁷ to ascertain its superiority. Additionally, the scoring model was validated at the pan-cancer level using the GEPIA2 website.

Association of the tryptophan metabolic risk score model with immune cell infiltration and related functions

The connection between risk scores and immune cell infiltration, as well as immune-related functions was investigated. The composition of 22 immune cell types in each tumor sample was quantified using the CIBERSORT algorithm²⁸. The differences in immune cell infiltration between high-risk and low-risk groups were then analyzed. Moreover, the correlation between the scoring model and immune cell infiltration was explored.

Correlation of the tryptophan metabolic risk score model with the tumor microenvironment and immune checkpoints

In the TME, immune-infiltrating cells, stromal cells, and tumor cells all contribute to tumor progression and drug resistance. Immune infiltration was analyzed using the “estimate” package²⁹, including Immune score, Stromal score, Tumor purity, and Estimate score. The expression of immune checkpoints (PD1, PDL1, CTLA4) in high-risk and low-risk patient groups was examined, and their correlation with the risk score model was explored.

Enrichment analysis and biological function annotation

To compare gene sets between high-risk and low-risk groups, Gene Set Enrichment Analysis (GSEA) was conducted using the gsea R package³⁰. Pathways with an adjusted P value < 0.05 were considered significantly enriched. Furthermore, Gene set variation analysis (GSVA) based on Hallmark gene sets was performed to assess the biological process status in the high-risk and low-risk groups³¹.

Screening of chemosensitive drugs

The “Oncopredict” R package was used to assess the sensitivity of different groups to various chemotherapy drugs³². By analyzing these differences, appropriate chemotherapy drugs for different patients were identified. Moreover, this approach serves to validate the clinical significance of the risk-scoring model.

Guiding significance of the tryptophan metabolism risk score model for immunotherapy

TIDE is a robust algorithm designed to assess tumor immune escape capacity, thereby predicting the efficacy of immune checkpoint blockade (ICB) therapy. A high TIDE score signifies a diminished response to ICB, whereas a low TIDE score suggests a favorable response^{33,34}. The TIDE database was utilized to scrutinize the variations in tumor immunotherapy responses across different tryptophan metabolism subgroups.

Validation of the heterogeneity of tryptophan metabolism in cancer at the single-cell level

Gene heterogeneity in the tryptophan metabolism pathway across different immune cell types in CC was investigated using the Tumor Immune Single-cell Hub (TISCH)¹⁷. The expression of risk model signature genes in epithelial cells was also examined using the single-cell tumor immune Microenvironment (scTIME) database³⁵. Additionally, single-cell RNA sequencing (scRNA-seq) was performed on four CRC samples. “Seurat” R package aided data preprocessing and dimensionality reduction. Cell clusters were identified with t-distributed stochastic neighbor embedding (t-SNE), and “SingleR” R package used CellMarker as a reference for cell annotation³⁶. “AUCell” R package gauged tryptophan metabolism gene activity. Interactions between epithelial cells and neighboring cells were studied with the “nichenetr” R package for ligand-receptor analysis, involving genes present in > 10% of cell clusters³⁷.

Statistical analysis

Data preprocessing and statistical analyses were conducted utilizing R software version 4.2.2. For continuous variables, the Wilcoxon rank-sum test was employed, while categorical variables were analyzed using the chi-square test. Statistical significance was determined with a two-tailed P value of less than 0.05. Heatmaps depicting eigengene expression were constructed using the ggplot2 package. Correlation analyses were performed employing the Pearson correlation coefficient. Survival analyses were visualized through Kaplan-Meier curves and assessed using the log-rank test.

Results

Genomic and transcriptomics changes of TMGs in CC

Forty tryptophan metabolism genes (TMGs) were collected from MSigDB and Reactome. We first assessed their changes at the genetic level in TCGA-COAD. As shown in the waterfall diagram (Fig. 1A), 123 out of 447 samples showed changes in tryptophan metabolism regulatory genes, among which the most common type of mutation was missense mutation, followed by nonsense mutation. The most commonly mutated genes were OGDH and OGDHL. Next, we investigated the CNV frequency mutations of TMGs. IDO1 and AFMID had a wide amplification in copy number. On the contrary, AADAT and IDO2 were focused on the prevalent CNV deletions (Fig. 1B). The location of CNV alterations of TMGs on chromosomes was demonstrated in Fig. 1C. Moreover, we explored differences in tryptophan metabolism genes at the transcriptome level, with 20 genes showing significantly different levels between tumor and normal samples ($p < 0.001$) (Fig. 1D). The activity of tryptophan metabolism genes also varied among different immune cell subsets. Consistent with the previous results, tryptophan metabolism genes were most significantly up-regulated in malignant cells, followed by fibroblasts (Fig.S1). These results indicated that TMGs had a large number of mutations and transcription differences in CC, suggesting that TMGs played an important role in the occurrence and development of CC.

Construction and verification of tryptophan metabolism risk score model

To gain a comprehensive view of the clinical significance of TMGs in CC, we performed a clustering analysis based on TMGs from TCGA-COAD. As shown, CC patients could be classified into two groups with distinct clinical heterogeneity and prognosis (Fig. 2A-C). Cluster2 patients had a worse prognosis than cluster1 patients (Fig. 2C). The results demonstrated that two different patterns did exist in CC. We found that patients with relatively advanced N stages were probably represented by cluster 2 (Fig. S7A). 16 survival-related genes were identified by univariate Cox regression analysis (Fig. S7B), and genes with importance scores greater than 10 were selected to construct the model (Fig. 2D-F). Five characteristic genes (NKAIN4, SLC16A8, UPK3B, PCOLCE2, TNNT1) were finally selected (Fig. 2F).

Next, we conducted validation across diverse cohorts employing the TMGs model. We stratified CC patients into high-risk and low-risk categories based on TMGs expression, revealing a substantial disparity in prognosis between the two cohorts. Within the TCGA dataset, patients with elevated risk scores experienced markedly inferior outcomes compared to those with lower risk scores ($P < 0.001$) (Fig. 3A). The model exhibited commendable discriminative ability, with high AUC values, effectively predicting survival rates at 1, 3, and 5 years (0.706, 0.703, and 0.689, respectively) (Fig. 3B). Notably, individuals classified in the high-risk group exhibited a heightened likelihood of mortality (Fig. 3C-D). Additionally, PCA and 3-dimensional PCA analyses exhibited a clear demarcation between the high and low-risk groups (Fig. 3E-F).

We then scrutinized the association with advanced clinical features and the score model. The correlations between the five characteristic genes of TMGs and clinical features were established (Fig. S2A). Elevated TMGs scores were notably prevalent among Cluster2 patients ($P < 0.001$), T4 patients ($P < 0.001$), N2 patients ($P < 0.001$), M1 patients ($P = 0.018$), and stage IV patients ($P = 0.012$) (Fig. S2B-F). These findings indicate a positive correlation between TMGs score and aggressive tumor behavior. Moreover, a comparative evaluation

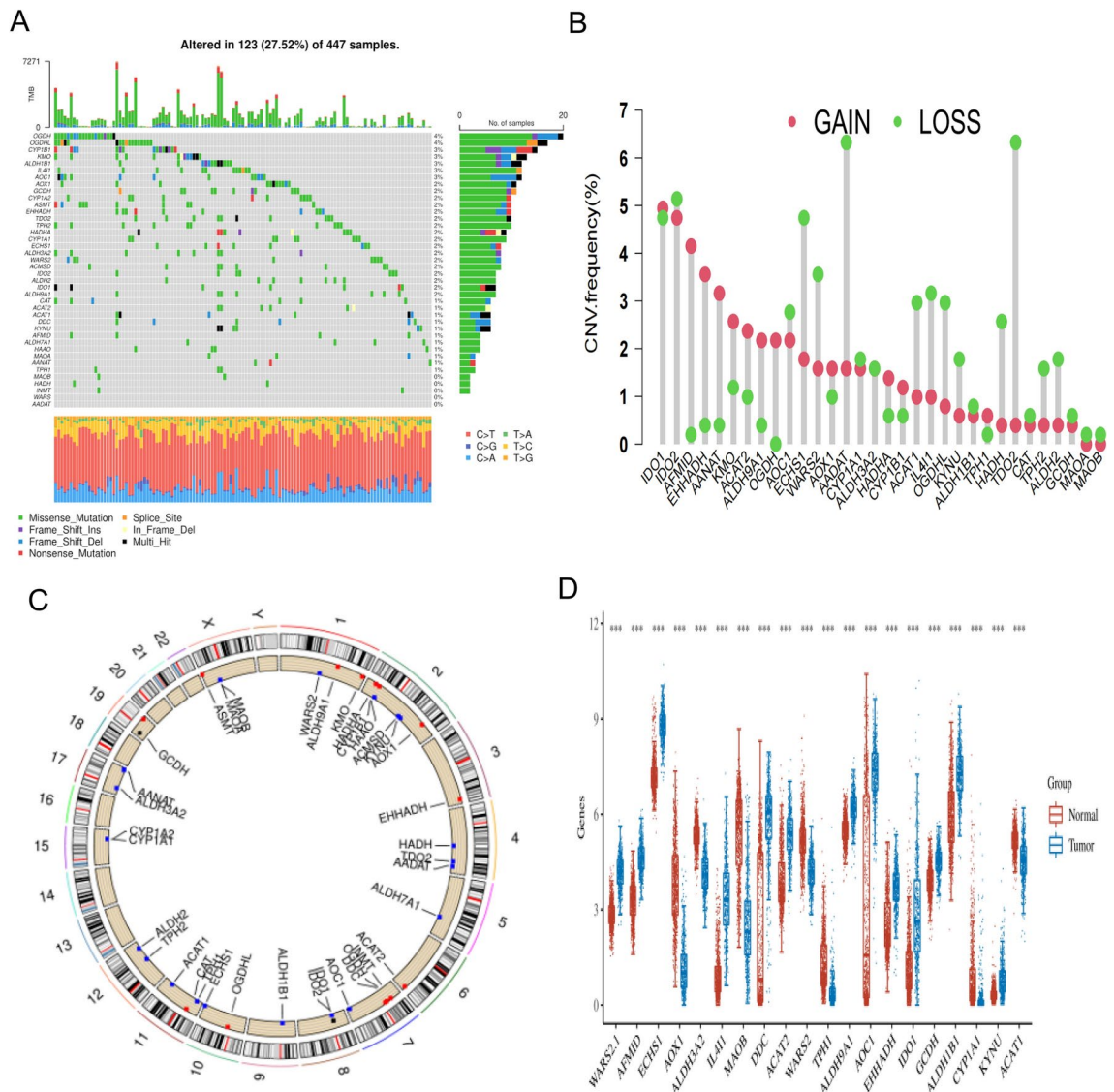


Fig. 1. Genetic and transcriptional alterations of tryptophan metabolism genes in colon cancer. **(A)** Frequency and type of mutations in tryptophan metabolism. **(B)** CNV mutations are widely found in the genes with tryptophan metabolism including gain or loss. **(C)** CNV alteration on chromosome of tryptophan metabolism from 1 to 22. **(D)** The mRNA expression levels of tryptophan metabolism genes in carcinoma and adjacent tissues in TCGA. CNV, Copy Number Variation.* $p < 0.05$, * $p < 0.01$ and *** $p < 0.001$.

between the TMGs model and four other CC scoring models confirmed the superior performance of our model, evidenced by a C-index value of 0.679 and HR=1.315 (95% CI: 1.226–1.411, $p < 0.001$) (Fig. S3A–B). Furthermore, results from the external cohort GSE38322 (Fig. 3G–L), GSE39582, GSE103479, GSE107797 (Fig. S4A–F), and the pan-cancer cohort (Fig. S5A–I) also validated the predictive power of our model.

Patients with different tryptophan metabolism risk scores have different signaling pathways and chemosensitivity drugs

To further investigate TMGs-related signaling pathways and biological functions, we performed Gene Set Enrichment Analysis (GSEA) and Gene Set Variation Analysis (GSVA). Cancer-promoting pathways and metabolic pathways were mainly concentrated in patients with high-risk scores, including WNT, Jak, Nod, and TGF, as well as β -alanine, and tryptophan metabolism (Fig. 4A,S8A). Immunoactivated pathways were enriched in patients with low-risk scores, including oxidative phosphorylation, peroxisome, ribosome function, and systemic lupus erythematosus (Fig. 4A,S8B). This is consistent with the results of higher expression of inhibitory immune cell infiltration in high-risk patients.

We extended our investigation to evaluate whether tryptophan metabolism similarly impacts chemotherapeutic responsiveness in CC patients. To this end, we employed the oncoPredict algorithm to predict the chemosensitivity of 198 therapeutic agents, determining their half-maximal inhibitory concentration (IC50) values and subsequently comparing these values between the high-risk and low-risk cohorts. Within the high-

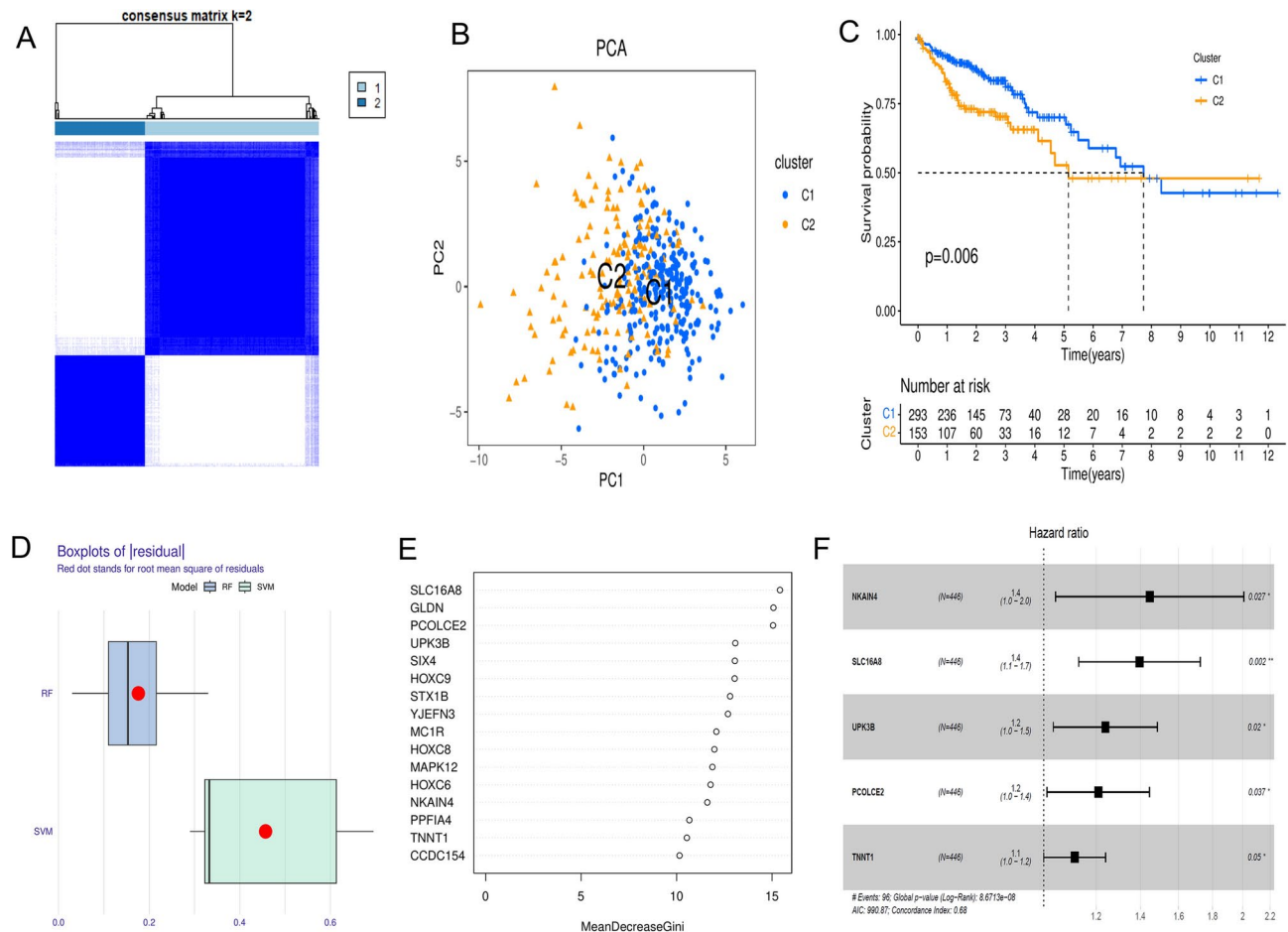


Fig. 2. Identification of tryptophan metabolic typing and scoring model construction in colon cancer. (A) When $K=2$, the component difference is obvious. (B) PCA analysis of the transcriptomic profiles of the two subtypes. (C) The difference of survival prognosis between the two subtypes was significant. (D) The RF algorithm is more stable than the SVM because of having lower residual values. (E) The random forest algorithm was used to select genes with an importance score greater than 10. (F) The forest plot shows the HR values and risk coefficient of risk score characteristic genes. PCA, Principal Component Analysis; RF, Random Forest; SVM, Support Vector Machine; HR, Hazard Ratio. * $p < 0.05$, ** $p < 0.01$ and *** $p < 0.001$.

risk group, patients demonstrated heightened sensitivity to three specific drugs, namely Erlotinib (Fig. 4B), Gefitinib (Fig. 4C), and SB505124 (Fig. 4D). Evidently, individuals classified within the high-risk category displayed pronounced sensitivity to these three chemotherapy agents. The potential clinical implications of these findings are substantial, particularly for treating refractory tumors and advancing the development and translation of targeted novel therapeutics. Furthermore, these outcomes offer valuable insights for guiding treatment stratification among CC patients.

TMGs regulate the immune microenvironment of CC

We further evaluated the effect of TMGs on the remodeling of TME of CC. Consistent with the oncogenic role of TMGs, the expression levels of inhibitory immune cells, such as regulatory T cells, M0 macrophages, and neutrophils, were increased in patients with a high tryptophan metabolic score (Fig. 5A). Furthermore, the expression levels of plasma cells and natural killer (NK) resting cells were significantly increased and the differences were statistically significant compared with patients with low tryptophan metabolic score ($p < 0.05$). In addition, TMGs showed a significant positive correlation with cytotoxic lymphocytes and endothelial cells ($p < 0.05$) (Fig. 5B). Substantial disparities emerged in key parameters such as ImmuneScore (Fig. 5C), StromalScore (Fig. 5D), Tumor purity (Fig. 5E), and ESTIMATE scores (Fig. 5F) between high and low-risk patients within the TCGA-COAD cohort. These findings suggest the possibility of varied responses to immunotherapy interventions based on distinct immune microenvironment characteristics.

Moreover, an investigation into immune checkpoint expression about high and low-risk cohorts demonstrated elevated levels of PDCD1, CD274, and CTLA4 within the high-risk group (Fig. 5G). Correlation analysis further revealed a positive association between the risk score and important immunotherapy-responsive markers such as PDCD1, CD274, CTLA4, IDO1, and TDO2 (Fig. 5H). Consequently, these results indicate a potential benefit of immune checkpoint inhibitors for high-risk individuals. To forecast the efficacy of immunotherapy, the TIDE

score was utilized to evaluate response in the high-risk group, yielding a significantly elevated score compared to the low-risk group (Fig. 5I). This suggests a heightened likelihood of immune escape and diminished immunotherapeutic response within the high-risk cohort. Furthermore, the high-risk group exhibited elevated levels of T-cell functional rejection and T-cell dysfunction relative to the low-risk group (Fig. 5J-K), also consistent with our results.

Single-cell sequencing data verifying the signature genes of the TMGs model

Utilizing single-cell sequencing data (GSE146771, EMTAB8107), we investigated tryptophan metabolism gene expression in diverse CC cell types. Employing dimensionality reduction and UMAP clustering analysis, we identified three cell subpopulations: immune, stromal, and malignant cells (Fig. S6A-B, E-F). In GSE179784, additional cell types including epithelial and dendritic cells were also annotated (Fig. S6I-J). Notably, TNNT1 and PCOLCE2 and UPK3B exhibited distinct expression within epithelial cells (Fig. S6C, G, K, D, H, L). Expression of other feature genes were summarized in Fig. S6D, H, L.

To further verify our theory, four matched CRC and normal samples were subjected to single-cell sequencing to achieve a high-resolution landscape of colorectal cancerous and normal tissue profiling. As shown, cells could be annotated as 8 clusters including T cells, epithelial cells, B cells, natural killer cells, monocytes, neutrophils, endothelial cells, and tumor stem cells (Fig. 6A-B). AUCell algorithm was then used to assess the tryptophan metabolism activity and distinguished the whole cell population as high and low subgroups (Fig. 6C-E). Consistent with the above results from bulk samples, AUC high and low groups differ in macrophages, neutrophils, and endothelial cells (Fig. 6F). These results may partly explain the different responses of patients in the TMGs-high and-low groups.

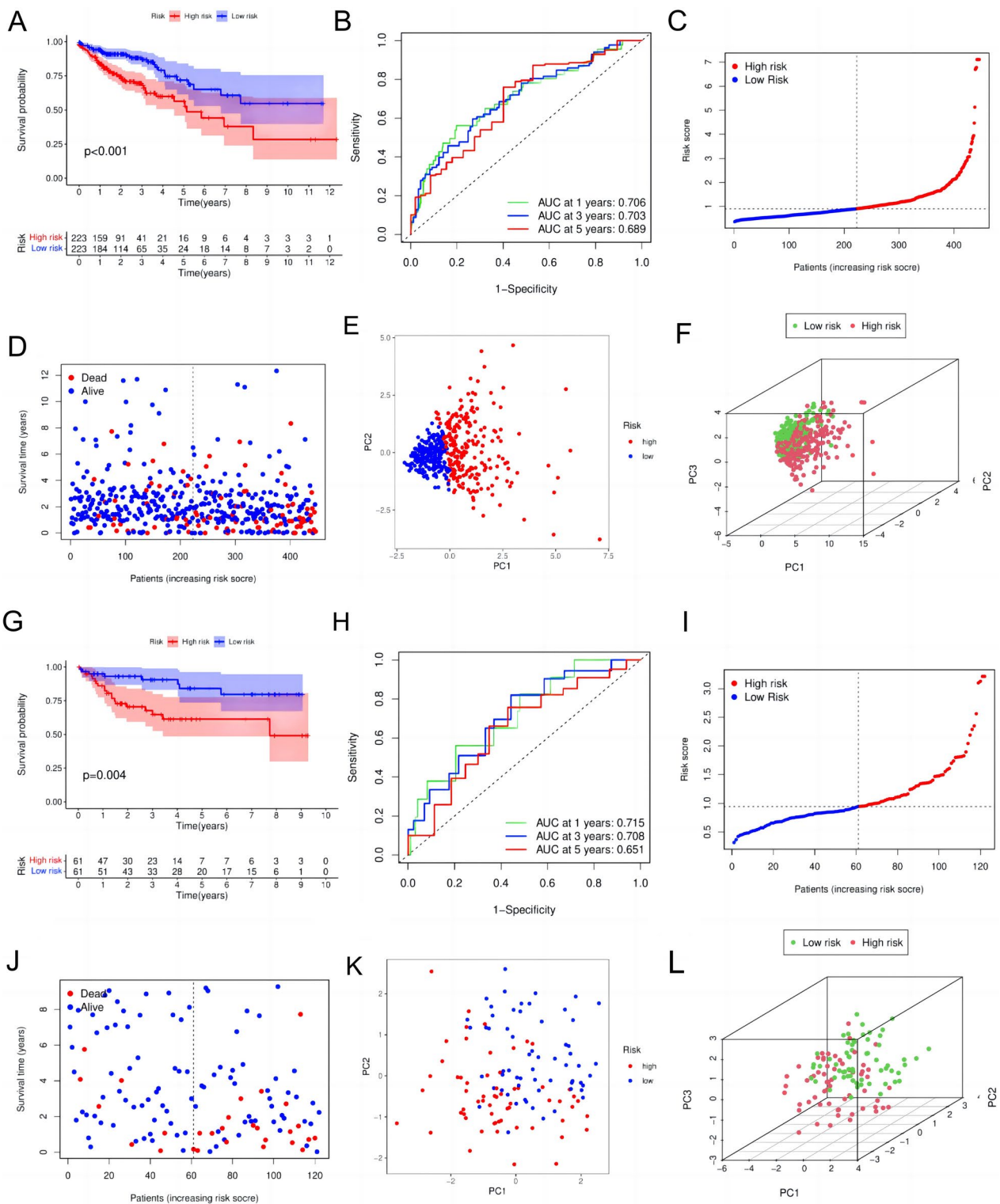
Moreover, cell-cell interaction was proved to be a key regulating factor of TME reprogramming and might play a crucial role in immune suppressive TME formation. In this study, we extracted multiple ligand-receptor pairs through the NicheNet algorithm. The results showed that there were activated signaling of TNF, VEGFC and EGFR from TMGs-high epithelial niches to endothelial cells (Fig. 7A-B), indicating hyperactivated angiogenesis in tumor stromal tissues and a potential response to VEGF blockage. Moreover, TMGs-high epithelial cells also released CXCL5, CXCL3, IL-1 to promote the infiltration of macrophages and neutrophils, which may also serve the formation of an immune suppressive TME. In addition, there were significant differences in metabolic pathways between the AUC_high group and the AUC_low group (Fig. 7C). Further molecular mechanisms were to be investigated by sub-clustering and analysis in the future.

Discussion

Current research highlights a strong correlation between the dysregulation of tryptophan metabolism and the onset of various cancers, including those of the esophagus, liver, and kidney^{38–40}. However, the specific mechanisms and molecular characteristics by which tryptophan metabolism influences CC remain largely unexplored. In this study, we stratified CC patients into two distinct subgroups based on the expression profiles of TMGs, each exhibiting unique molecular characteristics and clinical outcomes. The high-risk subgroup was characterized by reduced survival times and a diminished likelihood of benefiting from immunotherapy. Mechanistically, this subgroup displayed significant activation of metabolism-related pathways, including β -alanine metabolism, tryptophan metabolism, ECM receptor interactions, and chemokine signaling. Furthermore, immunosuppressive pathways such as TGF- β , JAK-STAT, and Notch were markedly upregulated in the high-risk group. Notably, β -alanine and tryptophan metabolism pathways have been associated with cancer cell proliferation and metastasis, likely by promoting metabolic reprogramming and immune escape. ECM receptor interactions and chemokine signaling pathways also play essential roles in CRC progression by enhancing cell invasion and migration. The activation of these pathways was strongly associated with tumor progression and poorer prognosis^{41–43}.

The TME comprises a complex network of blood vessels, immune cells, fibroblasts, inflammatory cells, signaling molecules, and the extracellular matrix that encases tumor cells. Tumors influenced this environment through signaling molecule release, angiogenesis, and immune tolerance⁴⁴. The intricate interplay between tumors and their immune microenvironment significantly shaped tumor progression and influenced treatment strategies⁴⁵. Based on the results of the KEYNOTE-177 clinical trial, ICB with or without typical chemotherapy, achieving an objective response rate of 41%, has become the first line treatment for metastatic CRC⁴⁶. In this study, we also analyzed the different TME contexts between high and low subgroups. As expected, high-risk cases were significantly enriched with immune-suppressive cells including Regulatory T cells (Treg), Cancer-Associated Fibroblasts (CAF), and INF γ , while low-risk cases possessed a more immune active TME, giving us a hint that these two groups might have varied responses to immunotherapy. Therefore, we performed preliminary validations in cohorts of cancer patients receiving adoptive T cell therapy or immune checkpoint blockade therapy and finally found out that TMGs active patients were less likely to respond to immune therapy, confirming that our model is a promising strategy to predict the survival and ICI therapeutic response. However, as profiling data of CRC cohorts receiving ICI treatment is still lacking, our model needs to be tested in CRC patients in the future.

To improve the treatment strategy of high-risk patients, we also screened possible effective drugs with the oncoPredict algorithm. Results showed that these patients might respond to erlotinib, gefitinib, and SB505124. Erlotinib and gefitinib are first and second-line therapies for non-small cell lung cancer, especially for lung cancer with metastatic EGFR mutation positive^{47,48}. In addition, both drugs have been studied extensively in other cancer fields. A phase III clinical trial (OPTIMOX3) showed that erlotinib combined with bevacizumab improves progression-free survival (PFS) in unresectable metastatic bowel cancer. Moreover, it has been found that gefitinib combined with cucurbitacin B inhibits the CRC cell cycle⁴⁹. Furthermore, Clinical studies hint at gefitinib's potential as a supplement to CC treatment⁵⁰. SB505124 is a novel small-molecule drug that is an



inhibitor of TGF β 1 receptors and is highly effective in cancer treatment. Studies have shown that SB505124 can reduce the expression of pro-angiogenesis genes in pancreatic cancer and inhibit angiogenesis *in vivo*⁵¹. Other studies have shown that the combination of SB505124 and IL-12 can effectively enhance anti-melanoma immunotherapy⁵². In addition, SB505124 could encapsulated in a targeted peptide and enhance natural killer (NK) cell anti-tumor activity for site-specific therapy⁵³. In addition, the study of this drug in bowel cancer is also worthy of our attention. SB-505124 has been reported to inhibit epithelial-mesenchymal transformation (EMT) in CRC cells⁵⁴. These findings merit further exploration, holding promise for refined treatment approaches in various cancers. This study's strengths include the establishment of a prognostic model based on robust machine learning algorithms and extensive validation across multiple external cohorts. However, the study has limitations, including its retrospective nature and reliance on publicly available datasets, which may introduce biases. Furthermore, the generalizability of the model needs to be validated in larger clinical cohorts.

Fig. 3. Validation of the risk score model in the TCGA and GEO independent cohorts. (A) Kaplan–Meier curve of OS in TCGA high-risk and low-risk patients. (B) The time-dependent ROC curve for the TCGA risk score. (C) The high-risk group of patients in the TCGA cohort had a high risk score (D) Patients in the high-grade group in the TCGA had lower survival days. (E) PCA showed that the TCGA high-risk and low-risk groups had identifiable dimensions. F 3dPCA showed that the TCGA high-risk group and the low-risk group can be well distinguished. (G) Kaplan–Meier curve of OS in GEO high-risk and low-risk patients. (H) The time-dependent ROC curve for the GEO risk score. (I) The high-risk group of patients in the TCGA cohort had a high risk score (J) Patients in the high-grade group in the TCGA had lower survival days. (K) PCA showed that the GEO high-risk and low-risk groups had identifiable dimensions (L) 3dPCA showed that the GEO high-risk group and the low-risk group can be well distinguished. OS, Overall Survival; TCGA, The Cancer Genome Atlas; ROC, Receiver Operating Characteristic Curve; PCA, Principal Component Analysis; 3dPCA, 3d Principal Component Analysis; GEO, Gene Expression Omnibus.

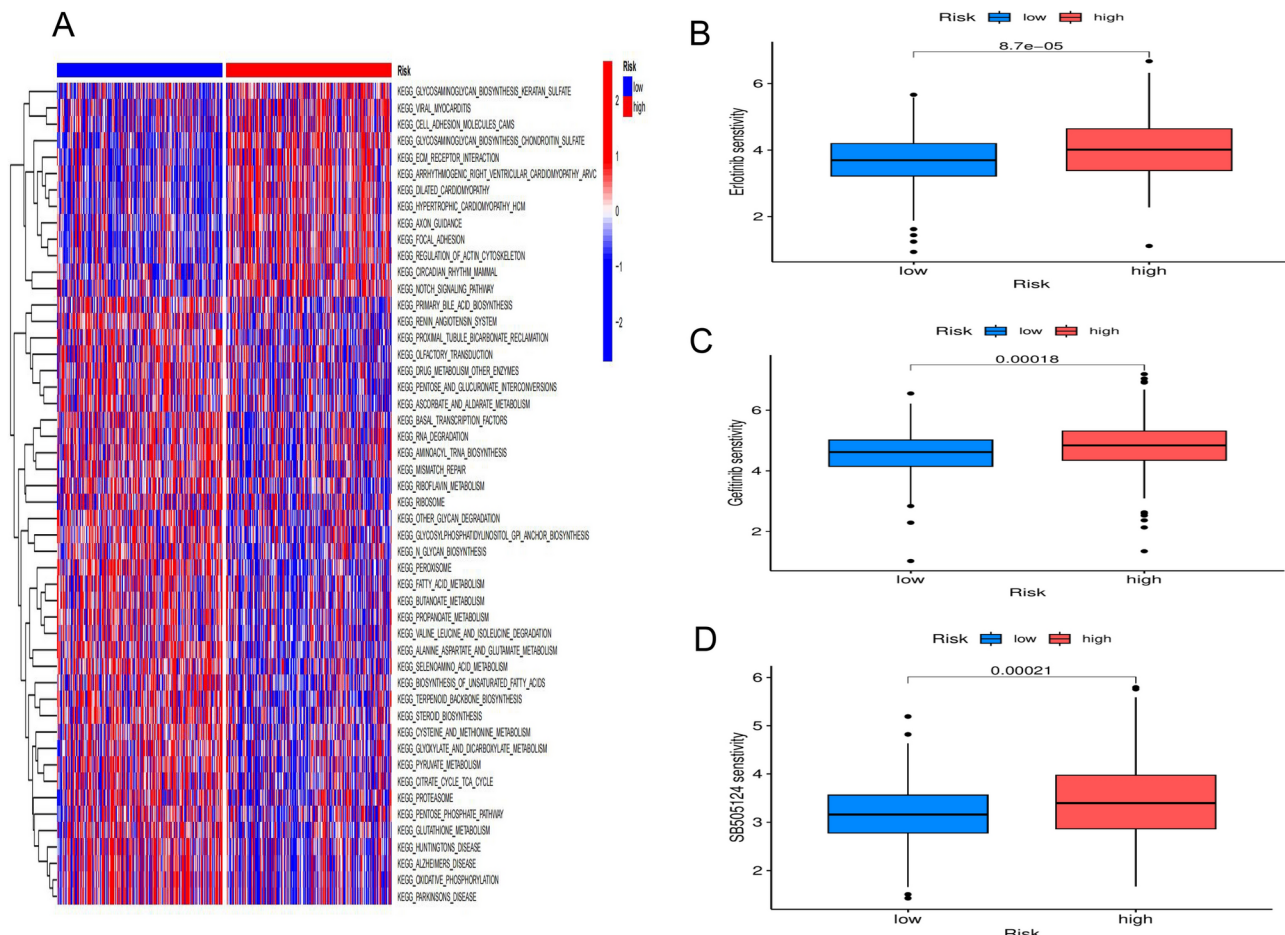


Fig. 4. Immune cell infiltration and functional differences and chemotherapy drug screening in the high-risk and low-risk groups. (A) GSVA enrichment analysis provides insights into the biological pathways and processes that are differentially activated or suppressed between the two groups. (B) The high-risk group had a high drug sensitivity for erlotinib. (C) The high-risk group had a high drug sensitivity for gefitinib. (D) The high-risk group had a high drug sensitivity for SB505124. GSEA, Gene-set enrichment analysis; GSVA, Gene set variation analysis.* $p < 0.05$, ** $p < 0.01$ and *** $p < 0.001$.

Conclusion

The findings of this study have significant clinical implications, particularly for the management of CC patients. The identification of distinct risk subgroups based on tryptophan metabolism provides a framework for personalized treatment strategies. The proposed TMGs risk score model can assist clinicians in predicting patient prognosis and optimizing therapeutic options, especially in the context of immunotherapy and targeted treatments. Overall, this study contributes valuable insights into the complex interplay between metabolism and cancer, highlighting potential avenues for future research and clinical application.

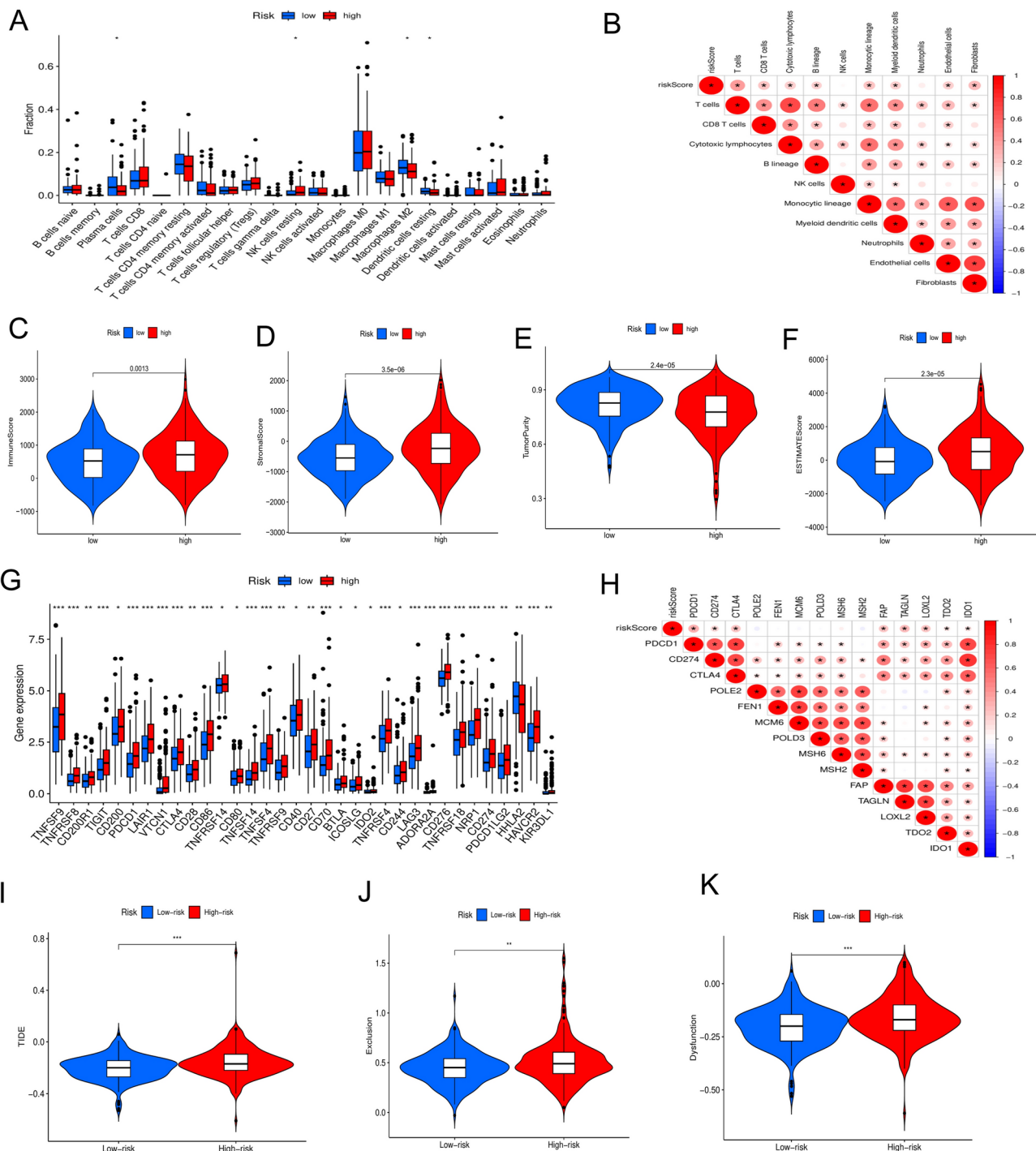


Fig. 5. Characteristics of the immune microenvironment and the prediction of immunotherapy in the high-risk and low-risk groups. (A) Differential analysis of tumor-infiltrating immune cells between high-risk groups and low-risk groups. (B) Correlation between the risk score model and tumor-infiltrating immune cells. (C) Immune score, (D) Stroma matrix score, (E) Tumor purity and (F) Estimate score between high-risk and low-risk groups. (G) Differential analysis of immune checkpoint between high-risk group and low-risk groups. (H) Correlation analysis between score model and immune checkpoint. (I) The TIDE score were higher in the high-risk group. (J) The T cell functional exclusion score were higher in the high-risk group. (K) The T cell dysfunction score were higher in the high-risk group. TIDE, Tumor immune dysfunction and rejection. * $p < 0.05$, ** $p < 0.01$ and *** $p < 0.001$.

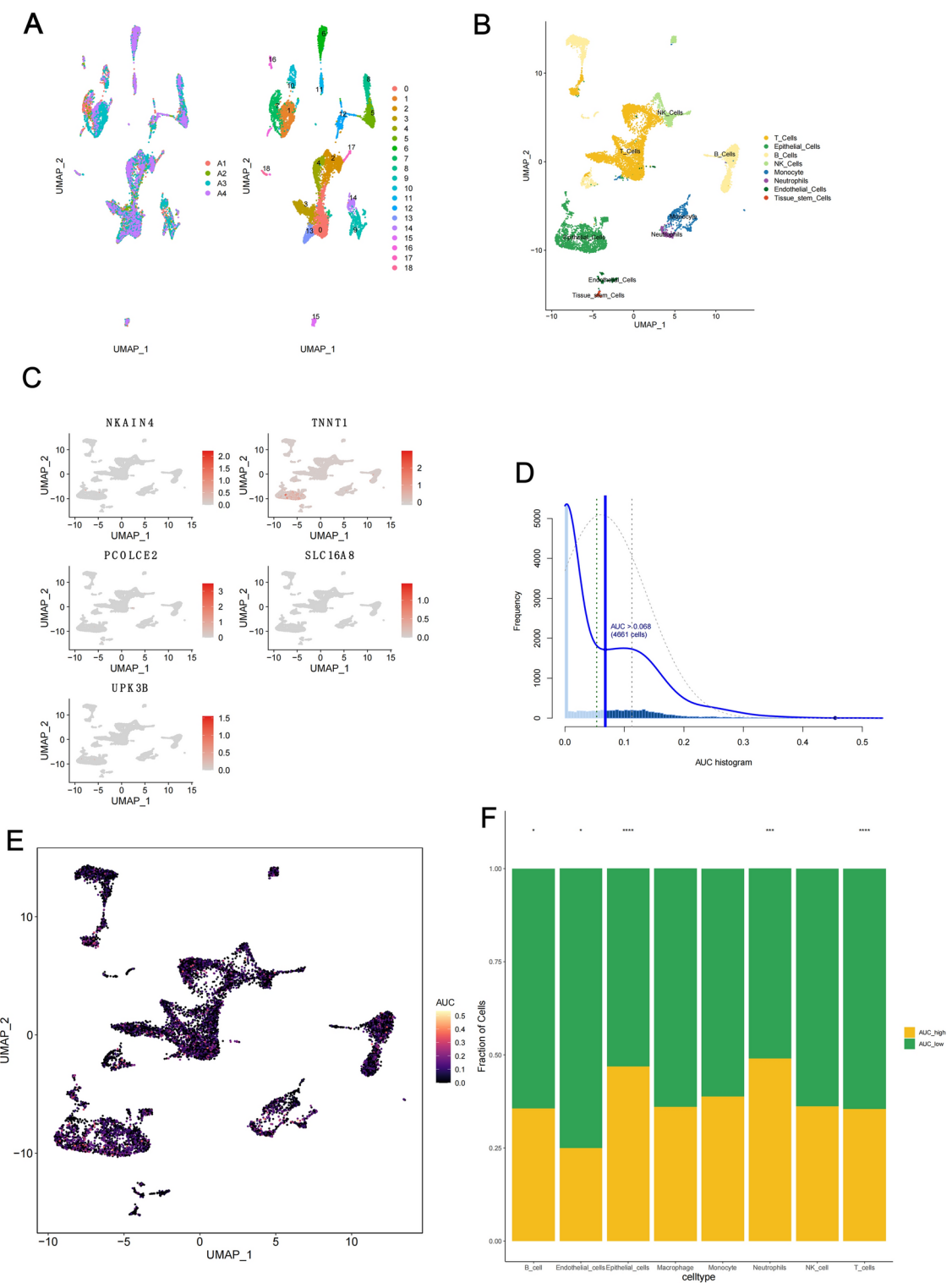
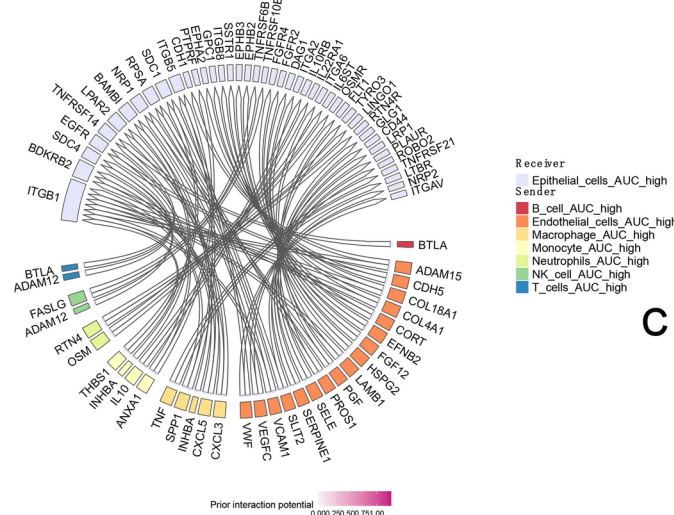
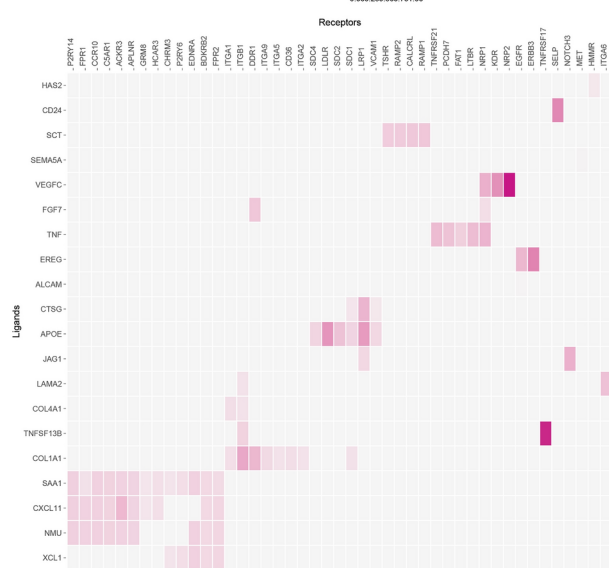


Fig. 6. Single-cell transcriptome analysis of the expression of signature genes for tryptophan metabolism in the tumor microenvironment. (A) Single-cell sequencing data of four intestinal cancer samples were combined and divided into 18 clusters. (B) After dimensionality reduction, the cluster cells are annotated as 8 cell subsets. (C) Expression activity of characteristic genes for tryptophan metabolism in epithelial cells. (D) The threshold was selected for 4661 cells at 0.068. (E) AUC score projection of tryptophan metabolism genes for all cells. (F) Stacked map of cell components in the AUC score group. AUC,area under the curve.* $p < 0.05$, ** $p < 0.01$ and *** $p < 0.001$.

A



B



C

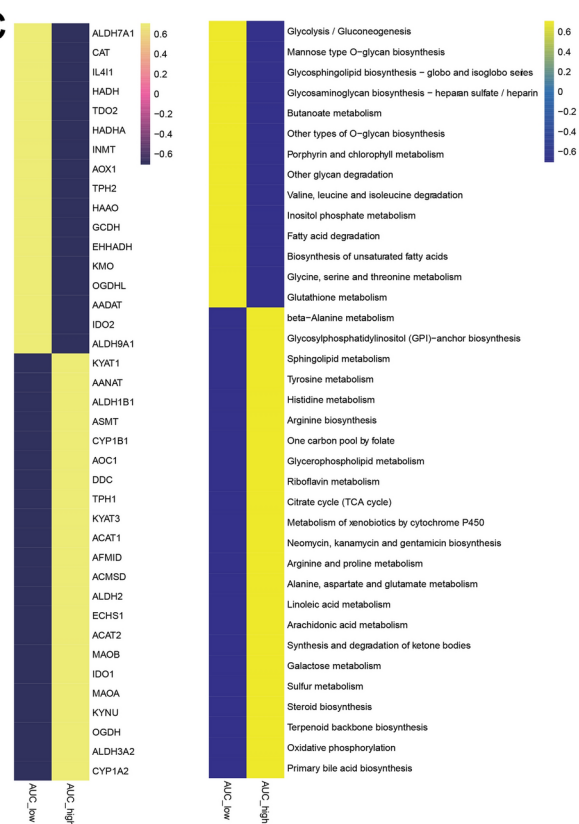


Fig. 7. Analyzes cell communication and pathway differences using single-cell data. (A) Circle diagram showing the interaction of ligand-target and ligand-receptor interactions. (B) Ligand receptor pairs reported in the network. (C) Differences in metabolic pathways between AUC_high and AUC_low groups. AUC,area under the curve.

Data Availability

The transcriptome data and related clinical data for 33 types of cancer were downloaded from the TCGA database (<https://cancergenome.nih.gov/>). Additional transcriptome sequencing and single-cell sequencing data can also be found in the GEO database (<https://www.ncbi.nlm.nih.gov/geo/>), TISCH database (<http://tisch.comp-genomics.org/>), GEPIA2 database (<http://gepia2.cancer-pku.cn/#index>), MSigDB database (<https://www.gsea-msigdb.org/gsea/msigdb/>), and TIDE database (<http://tide.dfci.harvard.edu/login/>). Any reasonable requests for access to available data underlying the results reported in this article will be considered. Such proposals should be submitted to the corresponding author.

Received: 13 July 2024; Accepted: 7 January 2025

Published online: 11 April 2025

References

1. Tan, S. et al. Exosomal cargos-mediated metabolic reprogramming in tumor microenvironment. *J. Exp. Clin. Cancer Res.* **42**(1), 59. <https://doi.org/10.1186/s13046-023-02634-z> (2023).
2. Nong, S. et al. Metabolic reprogramming in cancer: Mechanisms and therapeutics. *MedComm* **4**(2), e218. <https://doi.org/10.1002/mco2.218> (2023).
3. Wang, Z. et al. Amino acid metabolic reprogramming in tumor metastatic colonization. *Front. Oncol.* **13**, 1123192. <https://doi.org/10.3389/fonc.2023.1123192> (2023).

4. Sivanand, S. & Vander Heiden, M. G. Emerging roles for branched-chain amino acid metabolism in cancer. *Cancer Cell.* **37**(2), 147–156. <https://doi.org/10.1016/j.ccr.2019.12.011> (2020).
5. Chen, J. L. et al. The integrated bioinformatic analysis identifies immune microenvironment-related potential biomarkers for patients with gestational diabetes mellitus. *Front. Immunol.* **15**, 1296855. <https://doi.org/10.3389/fimmu.2024.1296855> (2024).
6. Li, X. & Zhang, H. S. Amino acid metabolism, redox balance and epigenetic regulation in cancer. *FEBS J.* **291**(3), 412–429. <https://doi.org/10.1111/febs.16803> (2024).
7. Xie, L. W. et al. Microbiota-derived I3A protects the intestine against radiation injury by activating AhR/IL-10/Wnt signaling and enhancing the abundance of probiotics. *Gut Microb.* **16**(1), 2347722. <https://doi.org/10.1080/19490976.2024.2347722> (2024).
8. Rad Pour, S. et al. Exhaustion of CD4+ T-cells mediated by the Kynureine Pathway in Melanoma. *Sci. Rep.* **9**(1), 12150. <https://doi.org/10.1038/s41598-019-48635-x> (2019).
9. Zhu, Q. N., Renaud, H. & Guo, Y. Bioinformatics-based identification of miR-542-5p as a predictive biomarker in breast cancer therapy. *Hereditas* **155**, 17. <https://doi.org/10.1186/s41065-018-0055-7> (2018).
10. Ala, M. Tryptophan metabolites modulate inflammatory bowel disease and colorectal cancer by affecting immune system. *Int. Rev. Immunol.* **41**(3), 326–345. <https://doi.org/10.1080/08830185.2021.1954638> (2022).
11. Xu, F. et al. Tryptophan As a New Member of RNA-Induced Silencing Complexes Prevents Colon Cancer Liver Metastasis. *Adv. Sci. (Weinh.)* **11**(31), e2307937. <https://doi.org/10.1002/advs.202307937> (2024).
12. Ning, J. Y. et al. Integrated network pharmacology and metabolomics reveal the action mechanisms of vincristine combined with celastrol against colon cancer. *J. Pharm. Biomed. Anal.* **239**, 115883. <https://doi.org/10.1016/j.jpba.2023.115883> (2024).
13. Routy, J. P. et al. The kynureine pathway is a double-edged sword in immune-privileged sites and in cancer: implications for immunotherapy. *Int. J. Tryptophan. Res.* **9**, 67–77. <https://doi.org/10.4137/IJTR.S38355> (2016).
14. Sun, X. Z. et al. Alteration of fecal tryptophan metabolism correlates with shifted microbiota and may be involved in pathogenesis of colorectal cancer. *World J. Gastroenterol.* **26**(45), 7173–7190. <https://doi.org/10.3748/wjg.v26.i45.7173> (2020).
15. Colaprico, A. et al. TCGAbioblinks: an R/Bioconductor package for integrative analysis of TCGA data. *Nucl. Acids Res.* **44**(8), e71. <https://doi.org/10.1093/nar/gkv1507> (2016).
16. Barrett, T. et al. NCBI GEO: archive for functional genomics data sets—update. *Nucl. Acids Res.* **41**, D991–D995. <https://doi.org/10.1093/nar/gks1193> (2013).
17. Sun, D. et al. TISCH: a comprehensive web resource enabling interactive single-cell transcriptome visualization of tumor microenvironment. *Nucl. Acids Res.* **49**(D1), D1420–D1430. <https://doi.org/10.1093/nar/gkaa1020> (2021).
18. Brinkman, E. K. & van Steensel, B. Rapid quantitative evaluation of crispr genome editing by TIDE and TIDER. *Methods Mol. Biol.* **1961**, 29–44. https://doi.org/10.1007/978-1-4939-9170-9_3 (2019).
19. Wilkerson, M. D. & Hayes, D. N. ConsensusClusterPlus: a class discovery tool with confidence assessments and item tracking. *Bioinformatics* **26**(12), 1572–1573. <https://doi.org/10.1093/bioinformatics/btq170> (2010).
20. Rigatti, S. J. Random forest. *J. Insur. Med.* **47**(1), 31–39. <https://doi.org/10.17849/insm-47-01-31-39.1> (2017).
21. Statnikov, A., Wang, L. & Aliferis, C. F. A comprehensive comparison of random forests and support vector machines for microarray-based cancer classification. *BMC Bioinform.* **9**, 319. <https://doi.org/10.1186/1471-2105-9-319> (2008).
22. Uddin, S. et al. Comparing different supervised machine learning algorithms for disease prediction. *BMC Med. Inform. Decis. Mak.* **19**(1), 281. <https://doi.org/10.1186/s12911-019-1004-8> (2019).
23. Ringner, M. What is principal component analysis?. *Nat. Biotechnol.* **26**(3), 303–304. <https://doi.org/10.1038/nbt0308-303> (2008).
24. Hong, J. et al. A Five-gene Signature for Predicting the Prognosis of Colorectal Cancer. *Curr. Gene. Ther.* **21**(4), 280–289. <https://doi.org/10.2174/156652322066201012151803> (2021).
25. Wang, S. et al. Screening and identification of immune-related genes for immunotherapy and prognostic assessment in colorectal cancer patients. *BMC Med. Genomics.* **15**(1), 177. <https://doi.org/10.1186/s12920-022-01329-2> (2022).
26. Ahluwalia, P. et al. Identification and Clinical Validation of a Novel 4 Gene-Signature with Prognostic Utility in Colorectal Cancer. *Int. J. Mol. Sci.* **20**, 15. <https://doi.org/10.3390/jims20153818> (2019).
27. Du, S. et al. Prognostic and therapeutic significance of a novel ferroptosis related signature in colorectal cancer patients. *Bioengineered.* **13**(2), 2498–2512. <https://doi.org/10.1080/21655979.2021.2017627> (2022).
28. Chen, B. et al. Profiling Tumor infiltrating immune cells with CIBERSORT. *Methods Mol. Biol.* **1711**, 243–259. https://doi.org/10.1007/978-1-4939-7493-1_12 (2018).
29. Yoshihara, K. et al. Inferring tumour purity and stromal and immune cell admixture from expression data. *Nat. Commun.* **4**, 2612. <https://doi.org/10.1038/ncomms3612> (2013).
30. Subramanian, A. et al. Gene set enrichment analysis: a knowledge-based approach for interpreting genome-wide expression profiles. *Proc. Natl. Acad. Sci. U.S.A.* **102**(43), 15545–15550. <https://doi.org/10.1073/pnas.0506580102> (2005).
31. Hanzelmann, S., Castelo, R. & Guinney, J. GSVA: gene set variation analysis for microarray and RNA-seq data. *BMC Bioinform.* **14**, 7. <https://doi.org/10.1186/1471-2105-14-7> (2013).
32. Maeser, D., Gruener, R. F. & Huang, R. S. oncoPredict: an R package for predicting in vivo or cancer patient drug response and biomarkers from cell line screening data. *Brief Bioinform.* **22**, 6. <https://doi.org/10.1093/bib/bbab260> (2021).
33. Fu, J. et al. Large-scale public data reuse to model immunotherapy response and resistance. *Genome. Med.* **12**(1), 21. <https://doi.org/10.1186/s13073-020-0721-z> (2020).
34. Jiang, P. et al. Signatures of T cell dysfunction and exclusion predict cancer immunotherapy response. *Nat. Med.* **24**(10), 1550–1558. <https://doi.org/10.1038/s41591-018-0136-1> (2018).
35. Hong, F. et al. Single-Cell Analysis of the Pan-Cancer Immune Microenvironment and scTIME Portal. *Cancer Immunol. Res.* **9**(8), 939–951. <https://doi.org/10.1158/2326-6066.CIR-20-1026> (2021).
36. Huang, Q. et al. Evaluation of cell type annotation r packages on single-cell RNA-seq Data. *Genom. Proteom. Bioinform.* **19**(2), 267–281. <https://doi.org/10.1016/j.gpb.2020.07.004> (2021).
37. Browaeys, R., Saelens, W. & Saeyns, Y. NicheNet: modeling intercellular communication by linking ligands to target genes. *Nat. Methods* **17**(2), 159–162. <https://doi.org/10.1038/s41592-019-0667-5> (2020).
38. Zhao, J. et al. A multi-platform metabolomics reveals possible biomarkers for the early-stage esophageal squamous cell carcinoma. *Anal. Chim. Acta.* **1220**, 340038. <https://doi.org/10.1016/j.aca.2022.340038> (2022).
39. Trezeguet, V., Fatrouni, H. & Merched, A. J. Immuno-metabolic modulation of liver oncogenesis by the tryptophan metabolism. *Cells.* **10**, 12. <https://doi.org/10.3390/cells10123469> (2021).
40. Cardenas, L. M. et al. Next wave of targets in the treatment of advanced renal cell carcinoma. *Curr. Oncol.* **29**(8), 5426–5441. <https://doi.org/10.3390/curoncol29080429> (2022).
41. Ma, W. et al. Kynureine produced by tryptophan 2,3-dioxygenase metabolism promotes glioma progression through an aryl hydrocarbon receptor-dependent signaling pathway. *Cell. Biol. Int.* **46**(10), 1577–1587. <https://doi.org/10.1002/cbin.11833> (2022).
42. Campia, I. et al. An Autocrine Cytokine/JAK/STAT-Signaling Induces Kynureine Synthesis in Multidrug Resistant Human Cancer Cells. *PLoS One.* **10**(5), e0126159. <https://doi.org/10.1371/journal.pone.0126159> (2015).
43. Park, J. H. et al. Kynureine promotes the goblet cell differentiation of HT-29 colon carcinoma cells by modulating Wnt Notch and AhR signals. *Oncol. Rep.* **39**(4), 1930–1938. <https://doi.org/10.3892/or.2018.6266> (2018).
44. Quail, D. F. & Joyce, J. A. The Microenvironmental landscape of brain tumors. *Cancer Cell* **31**(3), 326–341. <https://doi.org/10.1016/j.ccr.2017.02.009> (2017).
45. Quail, D. F. & Joyce, J. A. Microenvironmental regulation of tumor progression and metastasis. *Nat. Med.* **19**(11), 1423–1437. <https://doi.org/10.1038/nm.3394> (2013).

46. Diaz, L. A. Jr. et al. Pembrolizumab versus chemotherapy for microsatellite instability-high or mismatch repair-deficient metastatic colorectal cancer (KEYNOTE-177): final analysis of a randomised, open-label, phase 3 study. *Lancet. Oncol.* **23**(5), 659–670. [https://doi.org/10.1016/S1470-2045\(22\)00197-8](https://doi.org/10.1016/S1470-2045(22)00197-8) (2022).
47. Jung, H. A. et al. The Role of Brain Radiotherapy before First-Line Afatinib Therapy, Compared to Gefitinib or Erlotinib, in Patients with EGFR-Mutant Non-Small Cell Lung Cancer. *Cancer Res. Treat.* **55**(2), 479–487. <https://doi.org/10.4143/crt.2022.1344> (2023).
48. Yang, Z. et al. Comparison of gefitinib, erlotinib and afatinib in non-small cell lung cancer: A meta-analysis. *Int. J. Cancer* **140**(12), 2805–2819. <https://doi.org/10.1002/ijc.30691> (2017).
49. Yar Saglam, A. S. et al. Treatment with cucurbitacin B alone and in combination with gefitinib induces cell cycle inhibition and apoptosis via EGFR and JAK/STAT pathway in human colorectal cancer cell lines. *Hum. Exp. Toxicol.* **35**(5), 526–543. <https://doi.org/10.1177/0960327115595686> (2016).
50. Palumbo, I. et al. Gefitinib enhances the effects of combined radiotherapy and 5-fluorouracil in a colorectal cancer cell line. *Int. J. Colorectal. Dis.* **29**(1), 31–41. <https://doi.org/10.1007/s00384-013-1754-1> (2014).
51. Gore, J. et al. TCGA data and patient-derived orthotopic xenografts highlight pancreatic cancer-associated angiogenesis. *Oncotarget* **6**(10), 7504–7521. <https://doi.org/10.18632/oncotarget.3233> (2015).
52. Jiang, J. et al. Combined delivery of a TGF-beta inhibitor and an adenoviral vector expressing interleukin-12 potentiates cancer immunotherapy. *Acta Biomater.* **61**, 114–123. <https://doi.org/10.1016/j.actbio.2017.05.009> (2017).
53. Ximei, X. et al. Targeted anti-hepatocellular carcinoma research of targeted peptides combined with drug-loaded cell-derived microparticles. *J. Biomed. Nanotechnol.* **18**(4), 1009–1018. <https://doi.org/10.1166/jbn.2022.3311> (2022).
54. Jiang, Z. Y. et al. BMI-1 activates hepatic stellate cells to promote the epithelial-mesenchymal transition of colorectal cancer cells. *World J. Gastroenterol.* **29**(23), 3606–3621. <https://doi.org/10.3748/wjg.v29.i23.3606> (2023).

Acknowledgements

We are grateful to the patients for their contributions to this study.

Author contributions

Concept and design: XY, BF, JWJ. Funding acquisition and material support: BF, JWJ. Bioinformatics and single-cell sequencing analysis: YYH, XY, XMX. Manuscript writing and revision: YYH, XY, HZ. Data analysis assistance: CSD, SZ, WQ, EKZ, JPN, MQY. All authors have approved publication of the manuscript.

Funding

This study was supported by grants from the National Nature Science Foundation of China (NSFC) (Grant No. 82373237)

Declarations

Competing interests

The authors declare no competing interests.

Additional information

Supplementary Information The online version contains supplementary material available at <https://doi.org/10.1038/s41598-025-85893-4>.

Correspondence and requests for materials should be addressed to X.Y., B.F. or J.L.

Reprints and permissions information is available at www.nature.com/reprints.

Publisher's note Springer Nature remains neutral with regard to jurisdictional claims in published maps and institutional affiliations.

Open Access This article is licensed under a Creative Commons Attribution 4.0 International License, which permits use, sharing, adaptation, distribution and reproduction in any medium or format, as long as you give appropriate credit to the original author(s) and the source, provide a link to the Creative Commons licence, and indicate if changes were made. The images or other third party material in this article are included in the article's Creative Commons licence, unless indicated otherwise in a credit line to the material. If material is not included in the article's Creative Commons licence and your intended use is not permitted by statutory regulation or exceeds the permitted use, you will need to obtain permission directly from the copyright holder. To view a copy of this licence, visit <http://creativecommons.org/licenses/by/4.0/>.

© The Author(s) 2025